JBC Papers in Press. Published on February 26, 2019 as Manuscript RA119.007626
The latest version is at http://www.jbc.org/cgi/doi/10.1074/jbc.RA119.007626

Voltage-dependent activation in EAG channels follows a ligand-receptor rather than a mechanical-lever mechanism

Olfat A. Malak[1#], Grigory S. Gluhov[2], Anastasia V. Grizel[3], Kseniya S. Kudryashova[2, 4], Olga S. Sokolova[2,$], Gildas Loussouarn[1,$*]

Running Title: Voltage-dependent gating mechanism of EAG channels

[#] *present address: Cardiovascular Institute, Stanford University, 300 Pasteur Drive, Stanford, CA 94305-5111*

From the [1]INSERM, CNRS, l'Institut du Thorax, Université de Nantes, 44007, Nantes, France ; [2]Moscow M.V. Lomonosov State University, Moscow 119234, Russia;[3]Saint Petersburg State University, Saint Petersburg 199034, Russia; [4]Shemyakin-Ovchinnikov Institute of Bioorganic Chemistry of Russian Academy of Sciences, Moscow, 117997, Russia

[$] ***These authors contributed equally to this work.***

**To whom correspondence should be addressed:* Dr. Gildas Loussouarn, L'institut du thorax, INSERM UMR 1087 / CNRS UMR 6291, IRS-UN, 8 Quai Moncousu BP 70721, 44007 Nantes cedex 1, France; gildas.loussouarn@inserm.fr; Tel +33 (0)2 2808 0150

Keywords: EAG channel, K_V10.2 channel, voltage dependence, S4-S5 linker, S6 C-terminus, N-CAP, PAS domain, allostery, voltage-gated cation channel

ABSTRACT

Ether-a-go-go family (EAG) channels play a major role in many physiological processes in humans, including cardiac repolarization and cell proliferation. Cryo-EM structures of two of them, K_V10.1 and human ether-a-go-go-related gene (hERG or K_V11.1), have revealed an original non-domain–swapped structure, suggesting that the mechanism of voltage-dependent gating of these two channels is quite different from the classical mechanical-lever model. Molecular aspects of hERG voltage-gating have been extensively studied, indicating that S4-S5 linker (S4-$S5_L$) acts as a ligand binding to the S6 gate (S6 C-terminal part, $S6_T$) and stabilizing it in a closed state. Moreover, the N-terminal extremity of the channel, called N-Cap, has been suggested to interact with S4-$S5_L$ to modulate channel voltage-dependent gating, as N-Cap deletion drastically accelerates hERG channel deactivation. In this study, using COS-7 cells, site-directed mutagenesis, electrophysiological measurements, and immunofluorescence confocal microscopy, we addressed whether these two major mechanisms of voltage-dependent gating are conserved in K_V10.2 channels. Using cysteine bridges and S4-$S5_L$–mimicking peptides, we show that the ligand/receptor model is conserved in K_V10.2, suggesting that this model is a hallmark of EAG channels. Truncation of N-Cap domain, PAS domain, or both in K_V10.2 abolished the current and altered channel trafficking to the membrane, unlike for the hERG channel in which N-Cap and PAS domain truncations mainly affected channel deactivation. Our results suggest that EAG channels function via a conserved ligand/receptor model of voltage gating, but that the N-Cap and PAS domains have different roles in these channels.

Voltage-gated potassium (K_V) channels regulate a variety of cellular processes, including membrane polarization (1,2), apoptosis (3), cell

Downloaded from http://www.jbc.org/ by guest on February 27, 2019

proliferation (4), and cell volume (5). In connection with such a variety of functions of K_V channels, mutations in these channels cause a variety of pathological conditions in humans: neurological disorders (6,7), cardiac arrhythmias (2), multiple sclerosis (8), pain syndrome (9). It has also been shown, that K_V channels are associated with the development of malignant tumors cancer (10). K_V10 channels belong to the ether-a-go-go family (EAG), as hERG channels. Two isoforms of K_V10 channels are expressed in mammals: $K_V10.1$ (eag1) and $K_V10.2$ (eag2), which show 70% amino-acid sequence identity. $K_V10.1$ has been detected mainly in the brain, while $K_V10.2$ is also expressed in other tissues such as the skeletal muscles, the heart, the placenta, the lungs and the liver (11).

Atomic structures of rat $K_V10.1$ (12) and human hERG ($K_V11.1$) channels (13) highlighted many structural similarities: non-swapped pore and voltage domains *i.e.* facing voltage-sensor and pore domains are from the same subunit, short S4-S5 linkers (S4-$S5_L$) and similar N-terminal structures such as PAS and N-Cap domains. We hypothesized that molecular mechanisms of gating identified in hERG may apply to the closely related K_V10 channels.

In the heart, deactivation of hERG channels (closing of the activation gate) is slow, allowing a major role for this channel in the late repolarization phase of the action potential. In this channel, two mechanisms have been shown to play a major role in the deactivation process.

First, hERG deactivation is due to a voltage-dependent interaction between the S4-S5 region, including the S4-S5 linker and a part of S5 (named S4-$S5_L$, Figure 1A) and the C-terminal part of the S6 segment (named here $S6_T$), which is the activation gate (14,15). In other words, at resting potentials, S4-$S5_L$ (the ligand) is bound to the $S6_T$ gate (the receptor) and locks it in a closed state (as shown in Figure 1B left). Upon membrane depolarization, S4 drags S4-$S5_L$ out of the $S6_T$ gate, and the channel opens (Figure 1B middle). Upon repolarization S4-$S5_L$ binds to the $S6_T$ gate and channel deactivates (back to Figure 1B left). Here, using two distinct approaches, we observe that this ligand/receptor mechanism, which we originally proposed for hERG, is conserved in $K_V10.2$ (15).

Second, hERG deactivation is modulated by the channel N-terminus. In the N-terminal eag domain, deletion in the N-Cap and/or the PAS domains, profoundly accelerated deactivation with no major effect on maximal current amplitude (16-19). Moreover, covalent binding of the N-Cap and the S4-$S5_L$ closed the channel (20). These observations suggested that the N-Cap and/or the PAS domains regulate channel deactivation by modulating S4-$S5_L$ and $S6_T$ interaction. In $K_V10.2$, we show that eag domain presents quite different functions. Deletions of the N-Cap and PAS domains, separately or altogether, completely abolish channel activity, at least partially due to a defect in membrane trafficking.

In conclusion, we show that slowing activating channels follow an allosteric model, in which the voltage sensor and pore domains are weakly coupled, *via* a ligand, S4-$S5_L$ and a receptor, $S6_T$. In $K_V10.2$, such coupling is not modulated by the eag domain, as proposed for hERG (20).

Results

As in hERG, covalent binding of S4-$S5_L$ to $S6_T$ locks the $K_V10.2$ channel closed

The similar structures of hERG and $K_V10.1$ (12,13) showing a non-swapped arrangement of the pore and voltage sensor domains suggest that voltage-gating of these channels does not follow the classical mechanical-lever model in which S4-$S5_L$ constricts the $S6_T$ gate (21). Also, functional evidence obtained by several groups including ours, strongly suggests that hERG channels do not follow the mechanical-lever model (14,15). First, Ferrer and collaborators, observed that introduction of a cysteine in S4-$S5_L$ (D540C) and another cysteine in $S6_T$ (L666C) locks the channel in a closed state in oxidative condition. This was associated to a restricted movement of the voltage sensor in oxidative condition, as measured by gating currents, suggesting the formation of a disulfide bridge (14). Also, mutagenesis experiments on hERG suggested electrostatic interaction between D540 and L666 playing a major role in hERG voltage dependent gating (22). Such observations suggest that in the WT hERG channel, specific interactions between S4-$S5_L$ and

Downloaded from http://www.jbc.org/ by guest on February 27, 2019

the activation gate ($S6_T$) stabilize the closed channel. In transfected COS-7 cells, we could reproduce the experiments originally done by Ferrer and collaborators in the Xenopus oocyte model (15). Moreover we could observe that a S4-$S5_L$ mimicking peptide inhibits hERG channel, suggesting a ligand/receptor model, in which S4-$S5_L$, directly under the control of the voltage sensor S4, binds to $S6_T$ to lock the channel in a closed state (see Fig 1B, right).

In order to check whether K_V10.2 channels follow the same voltage-gating mechanism as hERG channels, we aligned the amino-acid sequences of the two channels, and mutated to a cysteine D339 and M474 in K_V10.2, corresponding to hERG positions in which cysteines were previously introduced: D540 in S4-$S5_L$ and L666 in $S6_T$ (14,15) (black arrows in Figure 1A). As for hERG double cysteine mutant, 2-hour application of 0.2 mM $tbHO_2$ led to an almost complete inhibition of the D339C-M474C K_V10.2 channel current (Figure 2A-B). Knowing the high homology between hERG and K_V10.2 (65 %), we supposed that D339C and M474C in K_V10.2 also form a disulfide bridge in oxidative condition, as a cause of the drastic current reduction. As control experiments, 0.2 mM $tbHO_2$ application had no effect on tail current amplitude when only one (D339C or M474C K_V10.2) or none (WT K_V10.2) of the two cysteines was introduced (Figure 2C-H) and activation curves showed a similar shift in all conditions (Supplemental Figure 1). Since a 2-hour $tbHO_2$ application represents a slow time course for a putative disulfide bridge formation, we also applied a higher concentration of $tbHO_2$ (2 mM) for a shorter time. As in Ferrer study on hERG, this concentration led, in around 12 minutes, to an almost complete inhibition of the D339C-M474C K_V10.2 channel current but not the WT channel current (Figure 3). This inhibition was reversed by 10mM DTT, as in Ferrer study on hERG.

To strengthen the hypothesis of the interaction between S4-$S5_L$ and $S6_T$ in K_V10.2, we also tested $tbHO_2$ effect on another double mutant of K_V10.2 channel. We chose E343C-M474C K_V10.2 channel, since E343, in S4-$S5_L$, is aligned with E544 in hERG which, when mutated to a cysteine together with L666C in hERG $S6_T$ (Figure 1A), also lead to channel inhibition, suggesting the formation of a disulfide bridge (15). We observed an inhibition of the current after 15' incubation of 2 mM $tbHO_2$, which is reversed by 10 mM DTT (Figure 4A-B). Control experiments showed no effect either on tail current amplitude or on the activation curve when only one (E343C or M474C K_V10.2) or none (WT K_V10.2) of the two cysteines was introduced (Figure 4C-H; Supplemental Figure 2). Altogether, these observations confirmed that two different disulfide bridges created between the two introduced cysteines in S4-$S5_L$ and $S6_T$ locks K_V10.2 in a closed state, as in hERG (14,15).

As in hERG, a K_V10.2 S4-$S5_L$ mimicking peptide inhibits K_V10.2 channels

Recently, we observed that (i) co-expressing a hERG S4-$S5_L$ mimicking peptide with hERG channel partially inhibited the generated current and (ii) covalently binding this peptide to the hERG channel completely inhibited it (15). These observations suggest that in hERG channels, S4-$S5_L$ rather acts as a voltage-controlled ligand that binds to the $S6_T$ gate and stabilizes it in the closed state (Figure 1B left for the endogenous interaction and 1B right for the mimicking peptide). This mechanism of gating is consistent with Ferrer et *al.* observation that covalent binding of S4-$S5_L$ and $S6_T$ channel regions locks the channel in a closed state (14). Using the alignment between hERG and K_V10.2 (Figure 1A), we designed the K_V10.2 S4-$S5_L$ peptide from the position of the S4-$S5_L$ peptide sequence that was inhibiting hERG channel (15). Co-expressing K_V10.2 channel with its specific S4-$S5_L$ peptide led to a profound decrease in current density (more than 70%), with no shift in the activation curve, as observed for hERG (Figure 5A-E). As an additional control, co-expressing K_V10.2 with a scramble S4-$S5_L$ peptide led to current density similar to the one observed in the absence of peptide (Figure 5A-B).

Since the S4-$S5_L$ peptide is supposed to interfere with the gating, it may be intriguing that activating and tail currents are inhibited to the same extent, and that neither the activation curve, nor the activation kinetics are modified (Figure 5C-F). To address this issue, we used a kinetic model mimicking the channel activity in presence/absence of the peptide (Figure 6), based on a previous model of KCNE1-KCNQ1 and S4-$S5_L$ peptide interaction (23). In KCNE1-KCNQ1

Downloaded from http://www.jbc.org/ by guest on February 27, 2019

model, the presence of the peptides was affecting the channel activation curve and activation kinetics. However, when constrained to K_V10.2 kinetics, the model did not show any alteration of activation kinetics or steady-state activation (Figure 6B-C). This is due to the fact that peptide binding and unbinding rates (0.02 and 0.04 s^{-1}, respectively) are lower than channel opening/closing rates, because increasing these rates leads to alterations in channel activation kinetics and steady-state activation (Figure 6B-C). A peptide with similar binding/unbinding rates impact KCNE1-KCNQ1 channel activation curve and activation kinetics (23) because gating kinetics of this channel are slower than K_V10.2 kinetics.

Altogether, these observations support the ligand/receptor model of voltage dependence in K_V10 channels.

As opposed to hERG, N-Cap and PAS domains deleted K_V10.2 channels are not functional

The results described above suggest that in both K_V10.2 and hERG channels, deactivation is due to S4-$S5_L$ binding to $S6_T$ and consequent stabilization of the closed state. It has been shown by several works that intracellular N-cap and PAS domains of hERG (shown in Figure 7A for K_V10.2, *cf.* alignment in Supplemental Figure 3) modulate channel deactivation kinetics. Most importantly truncated hERG channel missing N-Cap or the whole eag domain (N-Cap + PAS), when expressed in Xenopus oocytes, showed robust currents but a more than 5-fold acceleration in deactivation (16-19). Also in mammalian cells, it has been observed that eag domain is not necessary for hERG channel trafficking, consistent with the observation of robust currents in this model (24,25). Another work showed that N-Cap is close to S4-$S5_L$ (20). Thus, N-Cap may modulate channel deactivation through a direct interaction with this linker. Based on all these observations, we supposed that deletion of both N-Cap and PAS domains in K_V10.2 should give rise to functional channels with accelerated deactivation, as in the study on hERG in mammalian cells (25). Transfection of WT K_V10.2 tagged with 1D4 at the C-terminus gave rise to a current similar to previous description (6) and immunofluorescence experiments using this tag showed plasma membrane enrichment of the channel, compared to the intracellular compartment (Figure 7B-F). Surprisingly, deletion of N-Cap domain, PAS domain, but also of both domains all resulted in non-functional K_V10.2 channels (Figures 8B, 9B, 10B). Immunofluorescence experiments on N-Cap and/or PAS domains truncated channels showed no membrane enrichment of the channels (Figures 8C-F, 9C-F, 10C-F). These findings suggest a trafficking defect of the N-Cap and/or PAS domains truncated Kv10.2 channels.

As opposed to hERG, coexpressing a K_V10.2 N-Cap mimicking peptide with truncated K_V10.2 does not counteract the effect of channel truncation.

For hERG channel, it has been shown that a peptide corresponding to the first 16 amino acids of the channel is sufficient to reconstitute slow deactivation to hERG lacking this region (Wang et al 2000). Similarly, another study has shown that injection of the purified eag domain, corresponding to the first 135 amino acids of hERG, into oocytes expressing eag-truncated hERG, restores the deactivation kinetics to wild-type-like in more than 24 hours (Morais Cabral et al., 1998). Based on these previous observations on hERG, we proposed that co-expression of specific K_V10.2 N-Cap mimicking peptides with the N-Cap truncated K_V10.2 channel should recover its expression and activity at the plasma membrane. Surprisingly again, K_V10.2 channel activity was not recovered in the presence of N-Cap mimicking peptide (n=8). This observation further suggests that N-Cap and PAS domains play distinct roles in hERG and K_V10.2 function.

Co-expression of WT and truncated K_V10.2 channels gives rise to a right shift in the activation curve as compared to homomeric WT channels, but no change in deactivation kinetics.

In order to evaluate the potential effects of N-Cap truncation on channel activity, we co-expressed K_V10.2 missing the N-Cap with the WT channel, in an attempt to generate heteromers. We observed robust voltage-dependent currents, showing a ~30-mV shift in the activation curve towards depolarized potential, demonstrating the generation of such heteromers (Figure 11C-F). This shift in the activation curve suggests that N-Cap deletion leads not only to a K_V10.2 trafficking defect but also to a gating defect. In hERG channel, deletion of N-Cap did not lead to a shift

Downloaded from http://www.jbc.org/ by guest on February 27, 2019

of the activation curve, but an acceleration of deactivation (26). In the present experiments on K_V10.2, no change in deactivation kinetics was observed when the N-Cap truncated channel was co-expressed with the WT channel (Figure 12). We also co-expressed the K_V10.2 channel construct lacking both the N-Cap and PAS domains, with the WT channel. Again, we observed a ~30-mV shift in the activation curve towards depolarized potentials, but no modification in deactivation (Figures 11 & 12). Thus, although we are likely recording the combined activities of tetrameric channels containing different ratios of the WT and truncated subunits, it appears that N-terminal deletion of K_V10.2 impacts the steady-state activation curve rather than deactivation kinetics.

Discussion

From the present work and previous works, we suggest that among voltage-gated channels, coupling between voltage sensor movement and pore gating falls into two categories: (i) the mechanical-lever model: an obligatory coupling in which S4 resting state directly translates into S6 gate closed state. This mechanical-lever model, inferred from structural data in Shaker-like channels (27), also applies to eukaryotic sodium channels, as suggested by recent structural studies (28,29); (ii) the ligand/receptor model: the obligatory coupling cannot hold if the $S6_T$ gate is able to open, even if S4 segments are in the resting state, as shown for hERG and KCNQ1 channels (30-32), and, *vice-versa*, if $S6_T$ gate is able to close, even if S4 segments are in the activated state (33). We recently demonstrated this ligand/receptor model in hERG channels by using several approaches. Here, were obtained similar results on K_V10.2 using similar approaches.

First, introduction of cysteines in S4-$S5_L$ and $S6_T$, lock the channel in a closed state in oxidative condition, suggesting the formation of a disulfide bridge, as in hERG. This suggests that the same gating mechanism applies to K_V10.2. Introduction of cysteines in both S4-$S5_L$ and $S6_T$ may lead to a non-native conformation that favor an S4-$S5_L$ interaction with $S6_T$, which would not be met in WT channel. But in the second set of experiments, a S4-$S5_L$ mimicking peptide, without any introduced cysteine, inhibits K_V10.2 channel, also without any introduced cysteine, further suggesting the capability of S4-$S5_L$ to stabilize the channel closed state. Noteworthy, similar channel specific peptides have the same effect in KCNQ1 and hERG channels (15,23). Complementary experiments in hERG revealed that S4-$S5_L$ peptide effects was on channel gating, and not channel trafficking (15).

Altogether these experiments suggest that K_V10.2 follows the ligand/receptor mechanism observed in hERG. In both channels, S4-S5 linkers are short (12,13), thus it is likely that the part of S5 which is present in the peptide also plays a role in closed channel stabilization. Further structural data of hERG and K_V10.2 channels in the closed state should clarify the residues involved in the S4-$S5_L$ and $S6_T$ interaction. Noteworthy, this ligand/receptor model is consistent with the observation that the voltage-dependent closure of the related K_V10.1 channel, but also of the hERG channel, requires at least a part of the inhibiting S4-$S5_L$ to be covalently linked to the voltage sensor S4 (34,35).

As opposed to similar ligand/receptor gating mechanisms in the two channels, the role of the eag domain (N-Cap + PAS) is quite different between hERG and K_V10.2. In hERG channels, the eag domain (N-Cap + PAS) is not necessary for channel activity and mainly modulates the current deactivation rate (17-19). Here, we observed that truncation of K_V10.2 eag domain renders the channel nonfunctional, at least partly due to trafficking defects. In rescue experiments with the WT channel, we observed that eag domain deletion or even only N-Cap deletion are associated with a shift in the activation curve, but no change in channel deactivation. The contrary is observed in hERG channel: an altered deactivation, no shift in the activation curve (26,36). Our results suggest major differences in functional roles for the N-Cap and PAS domains between K_V10.2 and hERG. Altogether, this work suggests a conserved ligand/receptor (allosteric) model of voltage gating, but divergent roles in eag domains among channels of the EAG family.

In combination with a previous work on hERG, this study highlights in the voltage-gated channels superfamily, divergent gating mechanisms (obligatory *vs.* allosteric) that matches divergent structure (swapped vs non-swapped

Downloaded from http://www.jbc.org/ by guest on February 27, 2019

domain, respectively) and divergent kinetics (fast *vs.* slow activating channels, respectively). Non-swapped domains (hERG, K_V10) may provide less contact between S4-$S5_L$ and $S6_T$ (12,13). We propose that this weak coupling between S4-$S5_L$ and $S6_T$ provides a framework for a two-step channel activation: first, the fast S4 movement drags the ligand S4-$S5_L$ out of its receptor on the $S6_T$ gate, followed by slow gate opening. This allosteric regulation of the $S6_T$ gate by S4-$S5_L$ may explain how in slowly activating channels, movement of S4 is not concomitant to pore opening (37).

Experimental procedures

Plasmid constructs. pCDNA6 h$K_V10.2$ was subcloned into pMT3 vector using the standard PCR overlap extension method (38). A 1D4 immunoaffinity tag (derived from the C-terminus of bovine rhodopsin) was added to the C-terminus of all constructs (39). The D339C, E343C, M474C, E343C-M474C and D339C-M474C mutations were inserted into the pMT3-$K_V10.2$ construct using the Quikchange™ site directed mutagenesis-based techniques using Accuprime Pfx polymerase (ThermoFisher Scientific) according to the standard protocol recommended by the manufacturer. Truncation mutants were constructed by deleting residues 2 to 24 (ΔN-CAP), 2 to 134 (Δeag) and 25 to 134 (ΔPAS) using the standard PCR overlap extension method. PCR products were digested with HindIII and XbaI and ligated into pCDNA6 and PMT3 vectors. All constructs were confirmed by sequencing. Oligonucleotides encoding $K_V10.2$ peptides were synthesized by TOP Gene Technologies and contained a XhoI restriction enzyme, followed by a methionine (ATG) for translation initiation, a glycine (GGA) to protect the ribosome binding site during translation and the nascent peptide against proteolytic degradation (40). A BamHI restriction enzyme site was synthesized at the 3′ end immediately following the translational stop codon (TGA). These oligonucleotides were then ligated into pIRES2-EGFP (Clontech) and sequenced.

Cell culture and transfection. The African green monkey kidney-derived cell line COS-7 was obtained from the American Type Culture Collection (CRL-1651) and cultured in Dulbecco's modified Eagle's medium (GIBCO) supplemented with 10% fetal calf serum and antibiotics (100 IU/ml penicillin and 100 µg/ml streptomycin) at 5% CO_2 and 95% air, maintained at 37°C in a humidified incubator. Cells were transfected in 35-mm Petri dishes when the culture reached 50-60% confluence, with 4 µg total DNA complexed with 12 µl Fugene-6 (Roche Molecular Biochemical) according to the standard protocol recommended by the manufacturer. In the different experiments, plasmid quantities were optimized to keep current amplitudes in such a range, that undetectable currents were rare, and large currents inducing incorrect voltage-clamp were also rare. Immunofluorescence and confocal microscopy experiments were done with pCDNA6-$K_V10.2$ for which channel expression was lower than with pMT3-$K_V10.2$, to limit intracellular accumulation of the protein. For disulfide bridge experiments, COS-7 cells were co-transfected with 3.6 µg pMT3-WT or D339C-M474C or E343C-M474C or D339C or E343C or M474C $K_V10.2$ and 0.4 µg pEGFP. For S4-$S5_L$ peptide experiments, COS-7 cells were co-transfected with 2 µg pMT3-WT $K_V10.2$ and 2 µg pIRES2-EGFP plasmids encoding or not the S4-$S5_L$ peptide. As an additional control, a pIRES2-EGFP plasmid encoding a scramble S4-$S5_L$ peptide was used. In pIRES2-EGFP plasmids, the second cassette (EGFP) is less expressed than the first cassette, guaranteeing high levels of peptides expression in fluorescent cells (23). For N-terminal deletion experiments, COS-7 cells were co-transfected with 2 µg pCDNA6-N-Cap truncated $K_V10.2$ and 2µg pIRES2-EGFP plasmids encoding or not the N-Cap mimicking peptide. For immunofluorescence and confocal microscopy experiments, COS-7 cells were transfected with 4 µg pCDNA6-WT/truncated $K_V10.2$. For WT/truncated heteromeric $K_V10.2$ experiments, COS-7 cells were co-transfected with 1.8 µg pMT3-WT $K_V10.2$, 1.8 µg pMT3-truncated $K_V10.2$ and 0.4 µg pEGFP. Cells were re-plated onto 35-mm Petri dishes the day after transfection for patch-clamp experiments.

Electrophysiology. One day after splitting, COS-7 cells were mounted on the stage of an inverted microscope and constantly perfused by a Tyrode solution (cf. below) at a rate of 1-3 ml/min. The bath temperature was maintained at 22.0 ± 2.0°C. Stimulation and data recording were

Downloaded from http://www.jbc.org/ by guest on February 27, 2019

performed with Axon pClamp 10, an A/D converter (Digidata 1440A) and an Axopatch 200B amplifier (all Molecular Devices). Patch pipettes (tip resistance: 2–3 MOhms) were pulled from soda lime glass capillaries (Kimble-Chase) and coated with wax. Currents were recorded in the whole-cell configuration, pipette capacitance and series resistance were electronically compensated (by around 75%). Activation protocols were adjusted to the voltage-dependence of the construct as in the previous study on hERG (15). Activation curves were obtained from the tail currents and fitted by Boltzmann equations.

Confocal Microscopy. Immunohistological analyses were performed to study cell localization of transfected WT/truncated K_V10.2-1D4 in COS-7 cells. Twenty-four hours after transfection, cells were plated on IBIDI plates for 24 h. Cells were then fixed with 4% formaldehyde, stained for 10 minutes at room temperature with Alexa Fluor™ 647 Conjugated Wheat Germ Agglutinin (WGA; ThermoFisher), a plasma membrane marker, permeabilized with 0.5% saponin and blocked with 1% PBS-BSA. Cells were then incubated with a mouse monoclonal antibody directed against the 1D4 tag diluted in PBS (Abcam). Secondary antibody staining was performed using Alexa 488-conjugated anti-mouse antibody. DAPI was used for nuclear staining. Conventional imaging was performed using a LSM710-Confocor3 (Zeiss) and a Nikon Confocal A1RSi microscope system equipped with a SR Apo 100 × 1.49 N.A objective. Images were analyzed with Image J software. In figures, but not for analyses, Enhance Local Contrast adjustment was performed on WGA staining to highlight plasma membrane staining. To quantify fluorescence, the line plot was arbitrarily segmented in 3 different regions: the first and last 5-15% of the line plot, corresponding to plasma membrane (M1 and M2), and the remaining intermediate 70% of the line plot, corresponding to the intracellular compartment. For each of these regions in each cell, K_V10.2 fluorescence intensity values were normalized by the average cell K_V10.2 fluorescence intensity signal (41).

Solutions. Cells were continuously superfused with a HEPES-buffered Tyrode solution containing (in mmol/L): NaCl 145, KCl 4, $MgCl_2$ 1, $CaCl_2$ 1, HEPES 5, glucose 5, pH adjusted to 7.4 with NaOH. Patch pipettes were filled with the following solution (in mmol/L): KCl 100, K-gluconate 45, $MgCl_2$ 1, EGTA 5, HEPES 10, pH adjusted to 7.2 with KOH. For experiments in Figure 3, 1mM K_2ATP was added to limit current rundown. The membrane-permeable oxidizing agent tert-butylhydroperoxide ($tbHO_2$) was obtained from Sigma. Incubation of COS-7 cells with 0.2mM or 2mM $tbHO_2$ was realized at room temperature.

Kinetic model. The K_V10.2 kinetic model (Figure 6A top) contains two voltage sensor transitions, and two open states, as in the model of I_{Ks} (42). This model was optimized using IChMASCOT (J.A. De Santiago-Castillo and M. Covarrubias) to fit traces of the representative control of Figure 5. Optimized transition rates are presented in Table 1. Next, another model was designed (Figure 6A bottom), with an additional state in which S4-$S5_L$ mimicking peptide binds to the pre-open state and stabilizes it, as in (23). Various S4-$S5_L$ binding/unbinding transition rates were applied, and the effects on the biophysical parameters were studied.

Statistics. All data are expressed as means ± sem. Statistical differences between current densities (data points are not normally distributed) were determined using non parametric Mann Whitney test. Statistical differences between activation parameters, $V_{0.5}$, K (data points are normally distributed) were determined using unpaired Student's t-tests. A value of $p < 0.05$ was considered significant.

Downloaded from http://www.jbc.org/ by guest on February 27, 2019

Acknowledgments: We thank Isabelle Baró for careful reading of the manuscript. We thank the MicroPiCell facility of SFR Santé F. Bonamy for confocal microscopy experiments (Nantes).

Conflict of interest: The authors declare that they have no conflicts of interest with the contents of this article.

Author contributions: A.V.G. and G.S.G. carried out the mutagenesis. O.A.M. carried out the patch-clamp experiments. O.A.M., G.S.G. and K.S.K. carried out the confocal imaging experiments. O.A.M. analyzed the patch-clamp and confocal imaging experiments. G.L., O.S.S. and O.A.M. wrote the manuscript.

Reference List

1. Yellen, G. (2002) The voltage-gated potassium channels and their relatives. *Nature* **419,** 35-42

2. Charpentier, F., Merot, J., Loussouarn, G., and Baro, I. (2010) Delayed rectifier K(+) currents and cardiac repolarization. *J. Mol. Cell Cardiol.* **48,** 37-44

3. Pal, S., Hartnett, K. A., Nerbonne, J. M., Levitan, E. S., and Aizenman, E. (2003) Mediation of neuronal apoptosis by Kv2.1-encoded potassium channels. *J. Neurosci.* **23,** 4798-4802

4. Jimenez-Perez, L., Cidad, P., Alvarez-Miguel, I., Santos-Hipolito, A., Torres-Merino, R., Alonso, E., de la Fuente, M. A., Lopez-Lopez, J. R., and Perez-Garcia, M. T. (2016) Molecular Determinants of Kv1.3 Potassium Channels-induced Proliferation. *J. Biol. Chem.* **291,** 3569-3580

5. Piron, J., Choveau, F. S., Amarouch, M. Y., Rodriguez, N., Charpentier, F., Merot, J., Baro, I., and Loussouarn, G. (2010) KCNE1-KCNQ1 osmoregulation by interaction of phosphatidylinositol-4,5-bisphosphate with Mg2+ and polyamines. *J. Physiol* **588,** 3471-3483

6. Yang, Y., Vasylyev, D. V., Dib-Hajj, F., Veeramah, K. R., Hammer, M. F., Dib-Hajj, S. D., and Waxman, S. G. (2013) Multistate structural modeling and voltage-clamp analysis of epilepsy/autism mutation Kv10.2-R327H demonstrate the role of this residue in stabilizing the channel closed state. *J. Neurosci.* **33,** 16586-16593

7. Watanabe, H., Nagata, E., Kosakai, A., Nakamura, M., Yokoyama, M., Tanaka, K., and Sasai, H. (2000) Disruption of the epilepsy KCNQ2 gene results in neural hyperexcitability. *J. Neurochem.* **75,** 28-33

8. Judge, S. I. and Bever, C. T., Jr. (2006) Potassium channel blockers in multiple sclerosis: neuronal Kv channels and effects of symptomatic treatment. *Pharmacol. Ther.* **111,** 224-259

9. Beekwilder, J. P., O'Leary, M. E., van den Broek, L. P., van Kempen, G. T., Ypey, D. L., and van den Berg, R. J. (2003) Kv1.1 channels of dorsal root ganglion neurons are inhibited by n-butyl-p-aminobenzoate, a promising anesthetic for the treatment of chronic pain. *J. Pharmacol. Exp. Ther.* **304,** 531-538

Downloaded from http://www.jbc.org/ by guest on February 27, 2019

10. Pardo, L. A. and Stuhmer, W. (2014) The roles of K(+) channels in cancer. *Nat. Rev. Cancer* **14,** 39-48

11. Ju, M. and Wray, D. (2002) Molecular identification and characterisation of the human eag2 potassium channel. *FEBS Lett.* **524,** 204-210

12. Whicher, J. R. and Mackinnon, R. (2016) Structure of the voltage-gated K(+) channel Eag1 reveals an alternative voltage sensing mechanism. *Science* **353,** 664-669

13. Wang, W. and Mackinnon, R. (2017) Cryo-EM Structure of the Open Human Ether-a-go-go-Related K+ Channel hERG. *Cell* **169,** 422-430

14. Ferrer, T., Rupp, J., Piper, D. R., and Tristani-Firouzi, M. (2006) The S4-S5 linker directly couples voltage sensor movement to the activation gate in the human ether-a'-go-go-related gene (hERG) K+ channel. *J Biol. Chem.* **281,** 12858-12864

15. Malak, O. A., Es-Salah-Lamoureux, Z., and Loussouarn, G. (2017) hERG S4-S5 linker acts as a voltage-dependent ligand that binds to the activation gate and locks it in a closed state. *Sci. Rep.* **7,** 113

16. de la Pena, P., Machin, A., Fernandez-Trillo, J., Dominguez, P., and Barros, F. (2013) Mapping of interactions between the N- and C-termini and the channel core in HERG K+ channels. *Biochem. J* **451,** 463-474

17. Morais Cabral, J. H., Lee, A., Cohen, S. L., Chait, B. T., Li, M., and Mackinnon, R. (1998) Crystal structure and functional analysis of the HERG potassium channel N terminus: a eukaryotic PAS domain. *Cell* **95,** 649-655

18. Wang, J., Trudeau, M. C., Zappia, A. M., and Robertson, G. A. (1998) Regulation of deactivation by an amino terminal domain in human ether-a-go-go-related gene potassium channels. *J. Gen. Physiol* **112,** 637-647

19. Wang, J., Myers, C. D., and Robertson, G. A. (2000) Dynamic control of deactivation gating by a soluble amino-terminal domain in HERG K(+) channels. *J. Gen. Physiol* **115,** 749-758

20. de la Pena, P., Alonso-Ron, C., Machin, A., Fernandez-Trillo, J., Carretero, L., Dominguez, P., and Barros, F. (2011) Demonstration of physical proximity between the N terminus and the S4-S5 linker of the human ether-a-go-go-related gene (hERG) potassium channel. *J. Biol. Chem.* **286,** 19065-19075

21. Barros, F., Pardo, L. A., Dominguez, P., Sierra, L. M., and de la Pena, P. (2019) New Structures and Gating of Voltage-Dependent Potassium (Kv) Channels and Their Relatives: A Multi-Domain and Dynamic Question. *Int. J. Mol. Sci.* **20,**

22. Tristani-Firouzi, M., Chen, J., and Sanguinetti, M. C. (2002) Interactions between S4-S5 linker and S6 transmembrane domain modulate gating of HERG K+ channels. *J Biol. Chem.* **277,** 18994-19000

Downloaded from http://www.jbc.org/ by guest on February 27, 2019

23. Choveau, F. S., Rodriguez, N., Abderemane, A. F., Labro, A. J., Rose, T., Dahimene, S., Boudin, H., Le, H. C., Escande, D., Snyders, D. J., Charpentier, F., Merot, J., Baro, I., and Loussouarn, G. (2011) KCNQ1 channels voltage dependence through a voltage-dependent binding of the S4-S5 linker to the pore domain. *J Biol. Chem.* **286,** 707-716

24. Ke, Y., Hunter, M. J., Ng, C. A., Perry, M. D., and Vandenberg, J. I. (2014) Role of the cytoplasmic N-terminal Cap and Per-Arnt-Sim (PAS) domain in trafficking and stabilization of Kv11.1 channels. *J Biol. Chem.* **289,** 13782-13791

25. Fernandez-Trillo, J., Barros, F., Machin, A., Carretero, L., Dominguez, P., and de la Pena, P. (2011) Molecular determinants of interactions between the N-terminal domain and the transmembrane core that modulate hERG K+ channel gating. *PLoS. One.* **6,** e24674

26. Ng, C. A., Hunter, M. J., Perry, M. D., Mobli, M., Ke, Y., Kuchel, P. W., King, G. F., Stock, D., and Vandenberg, J. I. (2011) The N-terminal tail of hERG contains an amphipathic alpha-helix that regulates channel deactivation. *PLoS. One.* **6,** e16191

27. Long, S. B., Campbell, E. B., and Mackinnon, R. (2005) Voltage sensor of Kv1.2: structural basis of electromechanical coupling. *Science* **309,** 903-908

28. Shen, H., Zhou, Q., Pan, X., Li, Z., Wu, J., and Yan, N. (2017) Structure of a eukaryotic voltage-gated sodium channel at near-atomic resolution. *Science* **355,**

29. Yan, Z., Zhou, Q., Wang, L., Wu, J., Zhao, Y., Huang, G., Peng, W., Shen, H., Lei, J., and Yan, N. (2017) Structure of the Nav1.4-beta1 Complex from Electric Eel. *Cell* **170,** 470-482

30. Ma, L. J., Ohmert, I., and Vardanyan, V. (2011) Allosteric features of KCNQ1 gating revealed by alanine scanning mutagenesis. *Biophys. J* **100,** 885-894

31. Osteen, J. D., Barro-Soria, R., Robey, S., Sampson, K. J., Kass, R. S., and Larsson, H. P. (2012) Allosteric gating mechanism underlies the flexible gating of KCNQ1 potassium channels. *Proc. Natl. Acad. Sci. U. S. A* **109,** 7103-7108

32. Vardanyan, V. and Pongs, O. (2012) Coupling of voltage-sensors to the channel pore: a comparative view. *Front Pharmacol.* **3,** 145

33. Sun, J. and Mackinnon, R. (2017) Cryo-EM Structure of a KCNQ1/CaM Complex Reveals Insights into Congenital Long QT Syndrome. *Cell* **169,** 1042-1050

34. Tomczak, A. P., Fernandez-Trillo, J., Bharill, S., Papp, F., Panyi, G., Stuhmer, W., Isacoff, E. Y., and Pardo, L. A. (2017) A new mechanism of voltage-dependent gating exposed by KV10.1 channels interrupted between voltage sensor and pore. *J Gen. Physiol* **149,** 577-593

35. de la Pena, P., Dominguez, P., and Barros, F. (2018) Gating mechanism of Kv11.1 (hERG) K(+) channels without covalent connection between voltage sensor and pore domains. *Pflugers. Arch* **470,** 517-536

Downloaded from http://www.jbc.org/ by guest on February 27, 2019

36. Sale, H., Wang, J., O'Hara, T. J., Tester, D. J., Phartiyal, P., He, J. Q., Rudy, Y., Ackerman, M. J., and Robertson, G. A. (2008) Physiological properties of hERG 1a/1b heteromeric currents and a hERG 1b-specific mutation associated with Long-QT syndrome. *Circ. Res.* **103,** e81-e95

37. Goodchild, S. J. and Fedida, D. (2014) Gating charge movement precedes ionic current activation in hERG channels. *Channels (Austin.)* **8,** 84-89

38. Horton, R. M., Cai, Z., Ho, S. M., and Pease, L. R. (2013) Gene splicing by overlap extension: tailor-made genes using the polymerase chain reaction. BioTechniques 8(5):528-535 (November 1990). *Biotechniques* **54,** 129-133

39. Sokolova, O. S., Shaitan, K. V., Grizel', A. V., Popinako, A. V., Karlova, M. G., and Kirpichnikov, M. P. (2012) [Three-dimensional structure of human Kv10.2 ion channel studied by single particle electron microscopy and molecular modeling]. *Bioorg. Khim.* **38,** 177-184

40. Gilchrist, A., Li, A., and Hamm, H. E. (2002) G alpha COOH-terminal minigene vectors dissect heterotrimeric G protein signaling. *Sci. STKE.* **2002,** l1

41. Jouni, M., Si-Tayeb, K., Es-Salah-Lamoureux, Z., Latypova, X., Champon, B., Caillaud, A., Rungoat, A., Charpentier, F., Loussouarn, G., Baro, I., Zibara, K., Lemarchand, P., and Gaborit, N. (2015) Toward Personalized Medicine: Using Cardiomyocytes Differentiated From Urine-Derived Pluripotent Stem Cells to Recapitulate Electrophysiological Characteristics of Type 2 Long QT Syndrome. *J. Am. Heart Assoc.* **4,** e002159

42. Silva, J. and Rudy, Y. (2005) Subunit interaction determines IKs participation in cardiac repolarization and repolarization reserve. *Circulation* **112,** 1384-1391

43. Papadopoulos, J. S. and Agarwala, R. (2007) COBALT: constraint-based alignment tool for multiple protein sequences. *Bioinformatics.* **23,** 1073-1079

44. Thouta, S., Sokolov, S., Abe, Y., Clark, S. J., Cheng, Y. M., and Claydon, T. W. (2014) Proline scan of the HERG channel S6 helix reveals the location of the intracellular pore gate. *Biophys. J* **106,** 1057-1069

FOOTNOTES

This work was funded by the Kolmogorov program of the Partenariat Hubert Curien (35503SC) for Gildas Loussouarn and Olfat A. Malak and by Ministry of Education and Science of Russian Federation (RFMEFI61615X0044) for Olga S. Sokolova and Grigory S. Gluhov. Olfat A. Malak was laureate of the Line Pomaret-Delalande prize of the Fondation pour la Recherche Médicale (PLP20141031304; FRM). Olfat A. Malak wishes to personally thank Mrs. Line Pomaret for her generous support. Olfat A. Malak was supported by the Fondation Génavie. Grigory S. Gluhov was laureate of the Young Investigator award from Russian Scientific Foundation (18-74-00087). Anastasia Grizel was supported by Postdoctoral Fellowship from St. Petersburg State University (1.50.1038.2014) and grant from the Dynasty Foundation. LSM710-Confocor3 microscope was granted by the Moscow Lomonosov State University Program of Development.

Downloaded from http://www.jbc.org/ by guest on February 27, 2019

Table 1

Transition description		Transition rate (s^{-1})
Voltage sensor transition rates		
Closed Locked 2 (CL2) → Closed Locked 1 (CL1)	α	$8.50 \cdot \exp\left(0.14 \cdot \frac{V \cdot F}{R \cdot T}\right)$
CL1→ CL2	β	$13.35 \cdot \exp\left(-0.10 \cdot \frac{V \cdot F}{R \cdot T}\right)$
CL1 → Closed unlock (CU)	γ	$15.95 \cdot \exp\left(0.42 \cdot \frac{V \cdot F}{R \cdot T}\right)$
CU → CL1	δ	$4.12 \cdot 10^{-2} \cdot \exp\left(-0.76 \cdot \frac{V \cdot F}{R \cdot T}\right)$
Concerted opening transition rates		
4 monomers CU or CUP6 → Open state 1 (O1)	θ	$260.7 \cdot \exp\left(0.36 \cdot \frac{V \cdot F}{R \cdot T}\right)$
O1 → 4 monomers CU or CUP6	η	$64.66 \cdot \exp\left(-0.61 \cdot \frac{V \cdot F}{R \cdot T}\right)$
O1 → Open state 2 (O2)	ψ	$6.20 \cdot 10^{-3} \cdot \exp\left(2.37 \cdot \frac{V \cdot F}{R \cdot T}\right)$
O2 → O1	ω	$12.74 \cdot \exp\left(-2.46 \cdot \frac{V \cdot F}{R \cdot T}\right)$

F = 96485 C.mol-1 (Faraday constant); R = 8.314 J.mol-1.K-1 (Gas constant); T = 297 K; V (membrane potential) in V

Downloaded from http://www.jbc.org/ by guest on February 27, 2019

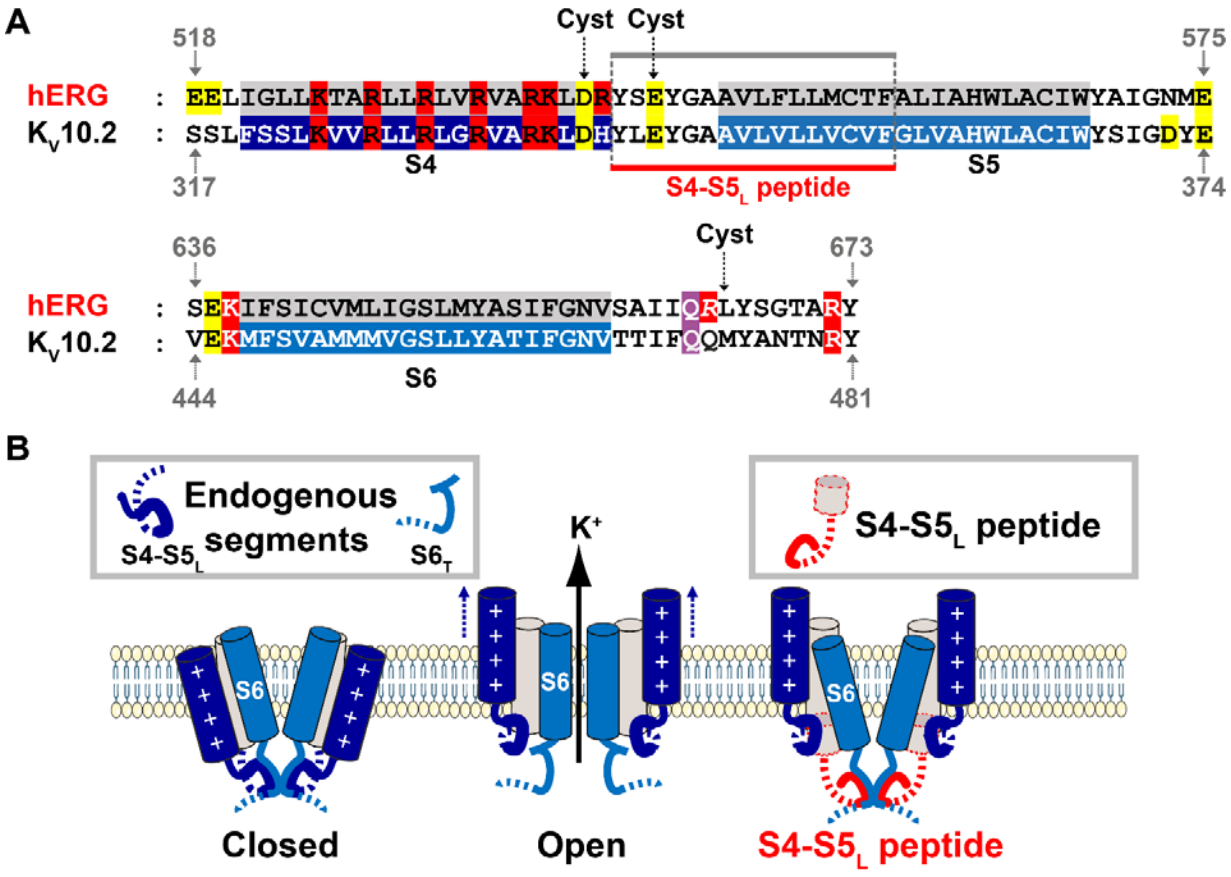

Figure 1: Alignment used to design the cysteine mutants and the S4-S5$_L$ peptide - hypothetical ligand/receptor model. A: alignment between hERG and K$_V$10.2. This alignment was used to (i) introduce the cysteines in S4-S5$_L$ and S6$_T$ and (ii) design the S4-S5$_L$ peptide from the previously identified hERG S4-S5$_L$ inhibiting peptide. S4-S5$_L$ refers to the S4-S5 region, including the S4-S5 linker and a part of S5. S6$_T$ refers to the C-terminal part of the S6 segment, which is the activation gate. The alignment was obtained using Cobalt (43). In red are represented the basic residues, in yellow acidic residues, and in purple the position of the narrowest part of the bundle crossing, also named the gating residue (44). The color boxes represent the transmembrane segments. Introduced cysteines in hERG (15) and in K$_V$10.2 in the present study are indicated. Grey line represents the inhibiting S4-S5$_L$ peptide in hERG (15). Red line represents the peptide engineered in K$_V$10.2 for the present study. **B. Left:** scheme of the hypothetical ligand/receptor model in which S4-S5$_L$ (deep blue) binds to S6$_T$ (light blue) to stabilize the channel in a closed state. **Middle**: upon membrane depolarization, S4 pulls S4-S5$_L$ out of the S6$_T$ receptor, allowing channel opening. **Right:** the K$_V$10.2 S4-S5$_L$ peptide (red) mimics endogenous S4-S5$_L$, locking the channel in its closed conformation.

Downloaded from http://www.jbc.org/ by guest on February 27, 2019

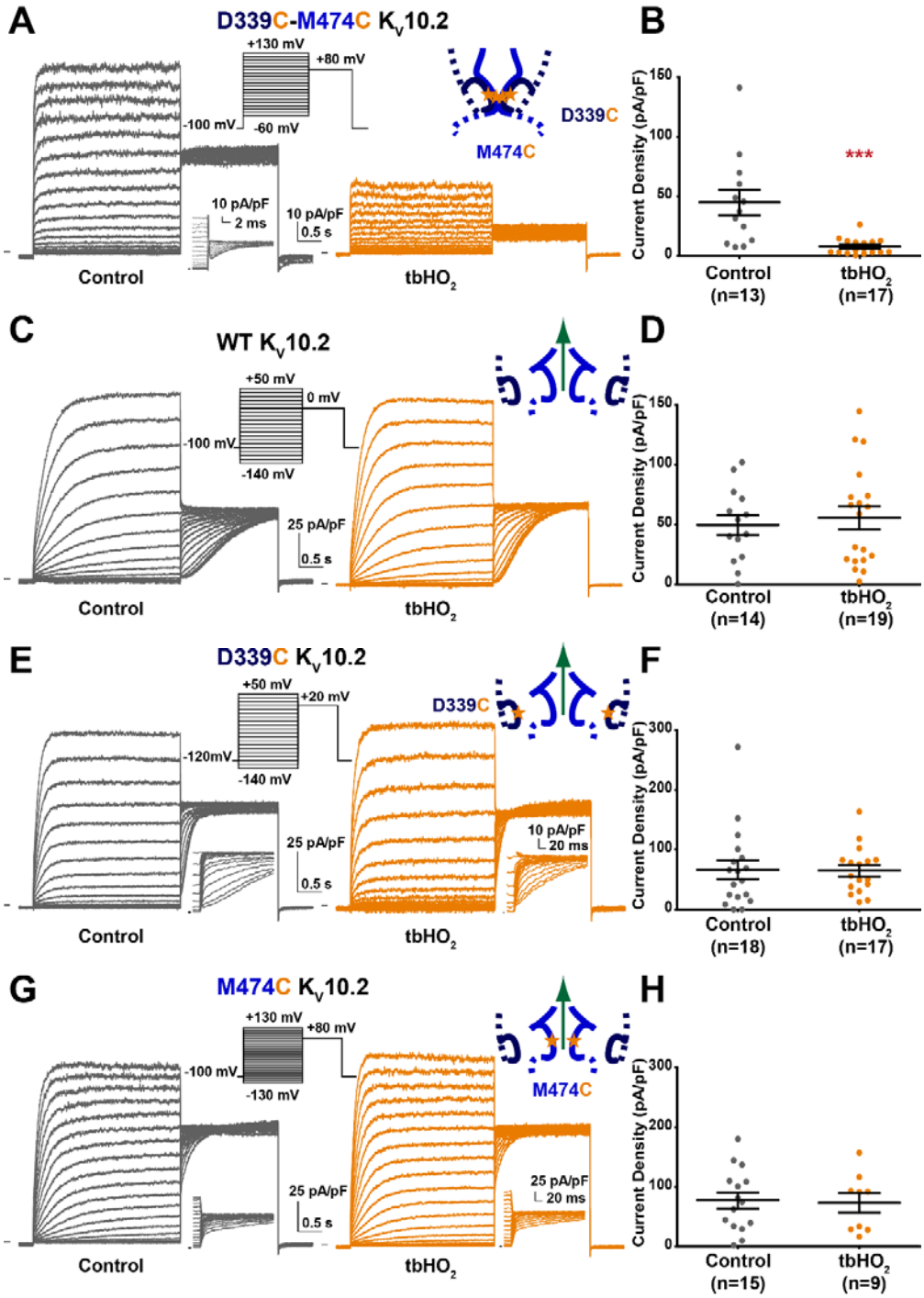

Figure 2: introduction of 2 cysteines in the S4-S5$_L$ and S6$_T$ regions of K$_V$10.2 (D339C-M474C K$_V$10.2) locks the channel closed in oxidative conditions. A: representative, superimposed recordings of the D339C-M474C K$_V$10.2 current after 2h incubation in Tyrode without (control) or with 0.2 mM tbHO$_2$ (tbHO$_2$). ***Left inset:*** activation voltage protocol used (one sweep every 8 s). ***Right inset*:** scheme of S4-S5$_L$/S6$_T$ with introduced cysteines (stars) **B:** mean ± sem D339C-M474C K$_V$10.2 maximum tail-current density, in control or tbHO$_2$. ***p<0.001 versus control, Mann-Whitney test. **C & D**: same as A & B for WT K$_V$10.2. **E & F**: same as A & B for D339C K$_V$10.2. **G & H**: same as A & B for M474C K$_V$10.2.

Downloaded from http://www.jbc.org/ by guest on February 27, 2019

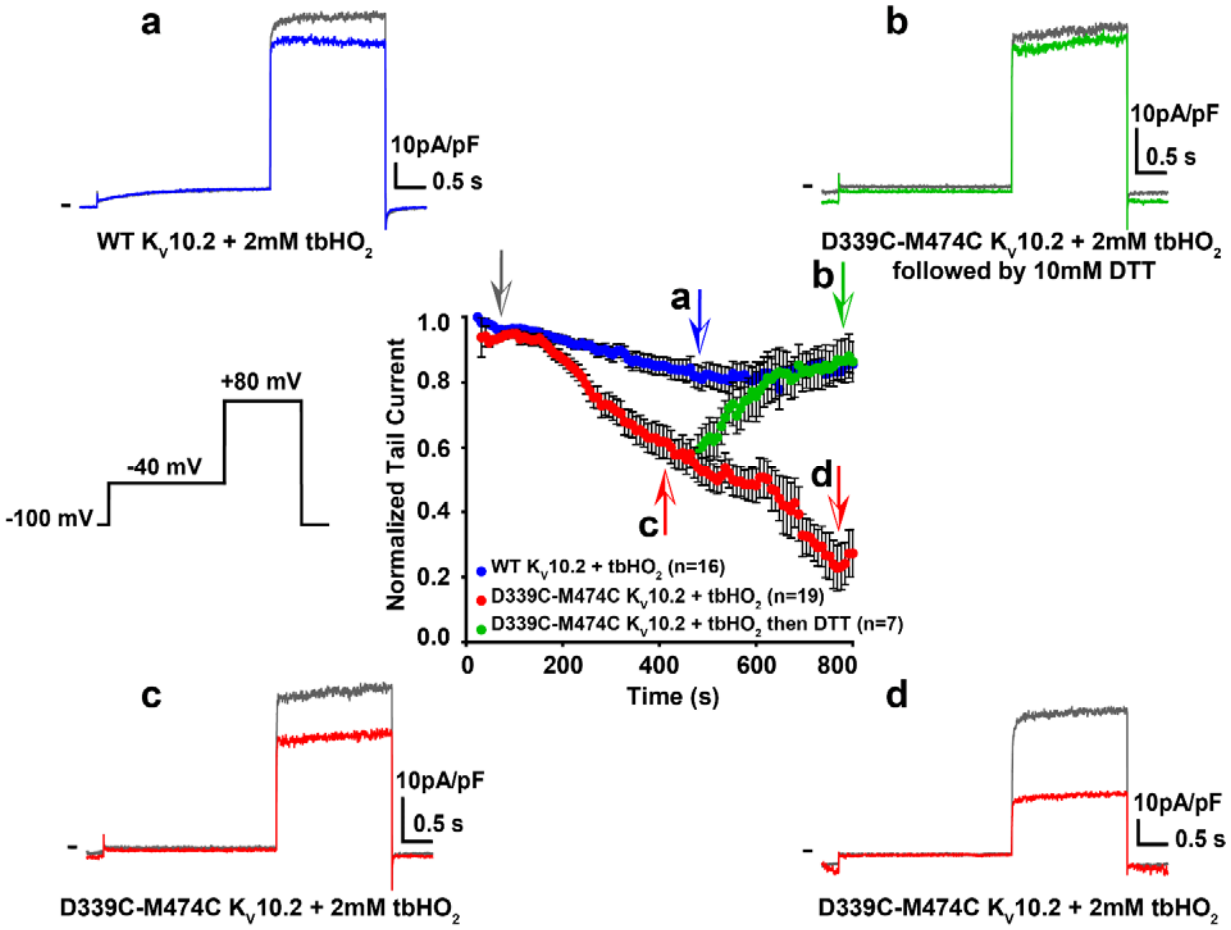

Figure 3: kinetics of D339C-M474C K_V10.2 current reduction upon addition of 2 mM $tbHO_2$. Time course of the effect of $tbHO_2$ application on normalized WT and D339C-M474C K_V10.2 tail currents. From a holding potential of -100mV, followed by a 3-s prepulse at -40 mV, tail currents were recorded at +80 mV, every 8 s. Following stabilization of the tail current, 2 mM $tbHO_2$ was perfused (grey arrow), and the step protocol was repeated for 6 min. Following the $tbHO_2$ application, a fraction of the cells was then perfused with 10 mM DTT, and the step protocol was continued for an additional 6 min. Each data point represents the mean ± sem current magnitude normalized to values obtained before $tbHO_2$. n = 16 (WT), 19 (D339C–M474C in $tbHO_2$), and 7 (D339C–M474C in DTT). Insets (a,b,c,d) corresponds to representative recordings at the arrows.

Downloaded from http://www.jbc.org/ by guest on February 27, 2019

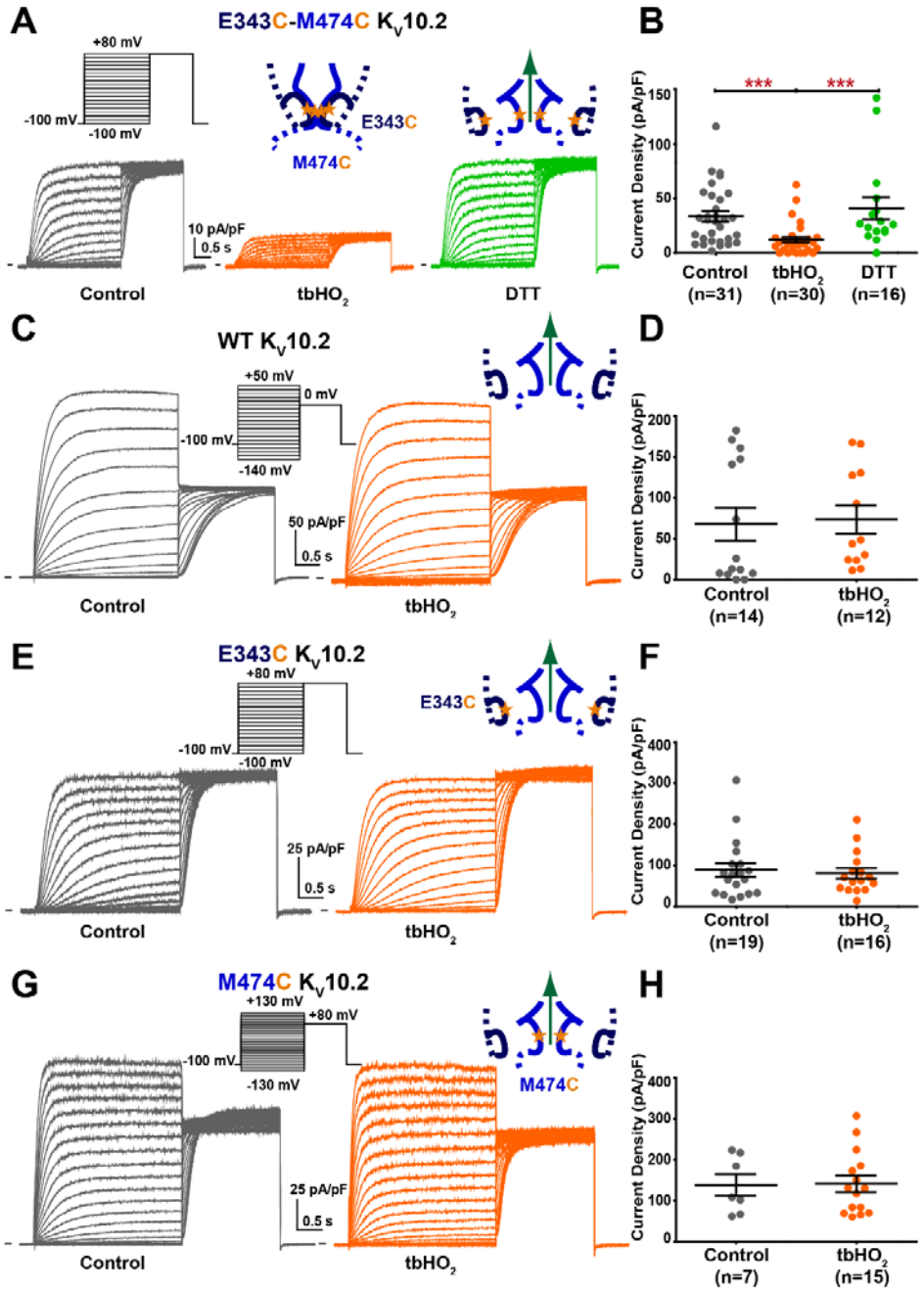

Figure 4: introduction of 2 cysteines in the S4-S5$_L$ and S6$_T$ regions of K$_V$10.2 (E343C-M474C K$_V$10.2) locks the channel closed in oxidative conditions. A: representative, superimposed recordings of the E343C-M474C K$_V$10.2 current after 15 min incubation in Tyrode without (control) or with 2 mM tbHO$_2$ (tbHO$_2$), or after subsequent 5 min incubation in 10 mM DTT (DTT). ***Left inset*:** activation voltage protocol used (one sweep every 8 s). ***Middle and right insets*:** Schemes of S4-S5$_L$/S6$_T$ with introduced cysteines in presence of tbHO$_2$ or DTT, respectively (stars). **B:** mean ± sem E343C-M474C K$_V$10.2 maximum tail-current density, in control, tbHO$_2$, or tbHO$_2$ followed by DTT. ***p<0.001, Mann-Whitney test. **C & D**: same as A & B for WT K$_V$10.2. **E & F**: same as A & B for E343C K$_V$10.2. **G & H**: same as A & B for M474C K$_V$10.2.

Downloaded from http://www.jbc.org/ by guest on February 27, 2019

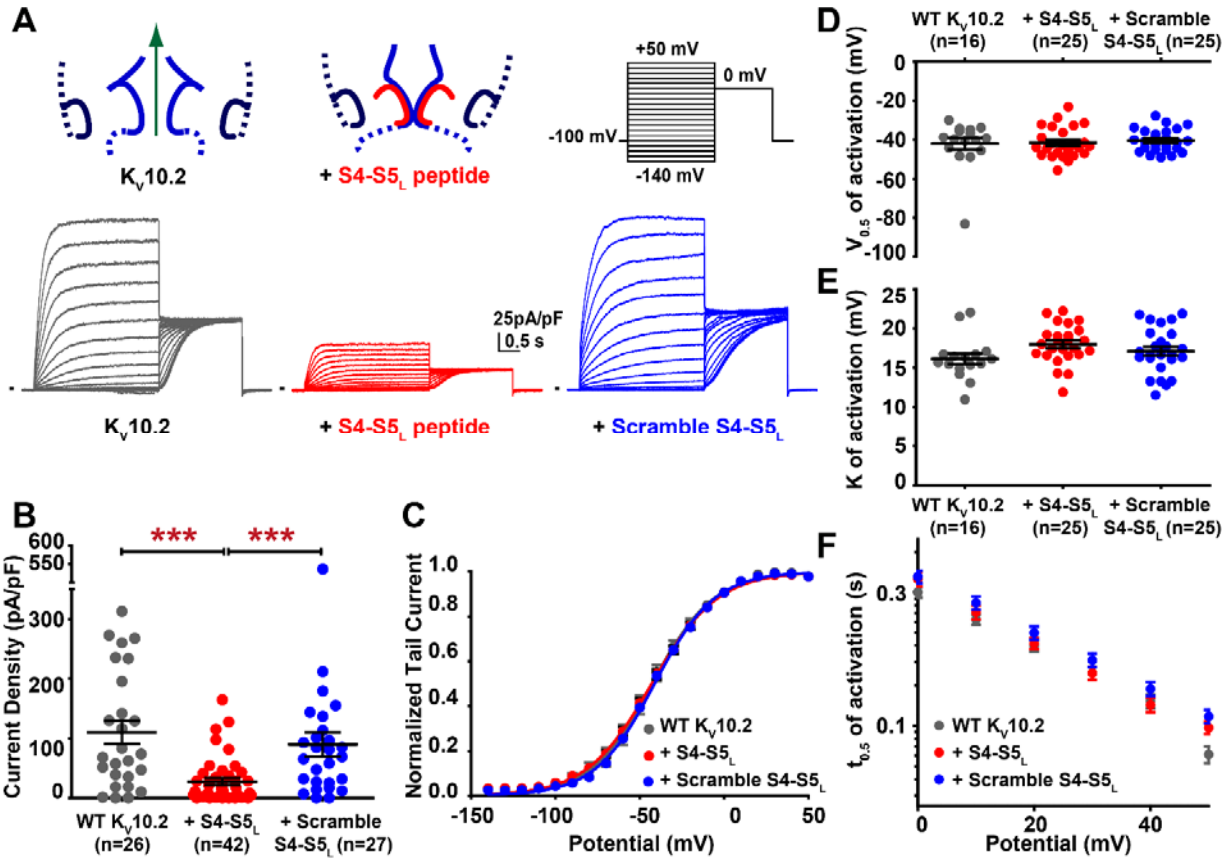

Figure 5: S4-S5$_L$ peptide inhibits K_V10.2 channels. A: representative, superimposed recordings of the WT K_V10.2 current in the absence (***left***; 2 µg K_V10.2 plus 2 µg GFP encoding plasmids), in the presence of S4-S5$_L$ peptide (***middle***; 2 µg K_V10.2 plus 2 µg peptide encoding plasmids) and in the presence of a scramble S4-S5$_L$ peptide (***right***; 2 µg K_V10.2 plus 2 µg peptide encoding plasmids). ***Left insets*:** schemes of the hypothetical effect of the S4-S5$_L$ inhibiting peptide on K_V10.2 channel; ***Right inset*:** activation voltage protocol used (one sweep every 8 s). **B**: mean ± sem K_V10.2 maximum tail-current density in the absence or presence of the indicated peptide (S4-S5$_L$ peptide or scramble S4-S5$_L$ peptide). ***p<0.001, Mann-Whitney test. **C**: activation curve, obtained from tail currents using the protocol shown in A, in the absence or the presence of the indicated peptide. (n=16-25). **D**: mean ± sem half-activation potential in the absence or the presence of the indicated peptide. **E:** mean ± sem activation curve slope in the absence or the presence of the indicated peptide. **F:** mean ± sem half-activation time as a function of membrane potential, in the absence or the presence of the indicated peptide.

Downloaded from http://www.jbc.org/ by guest on February 27, 2019

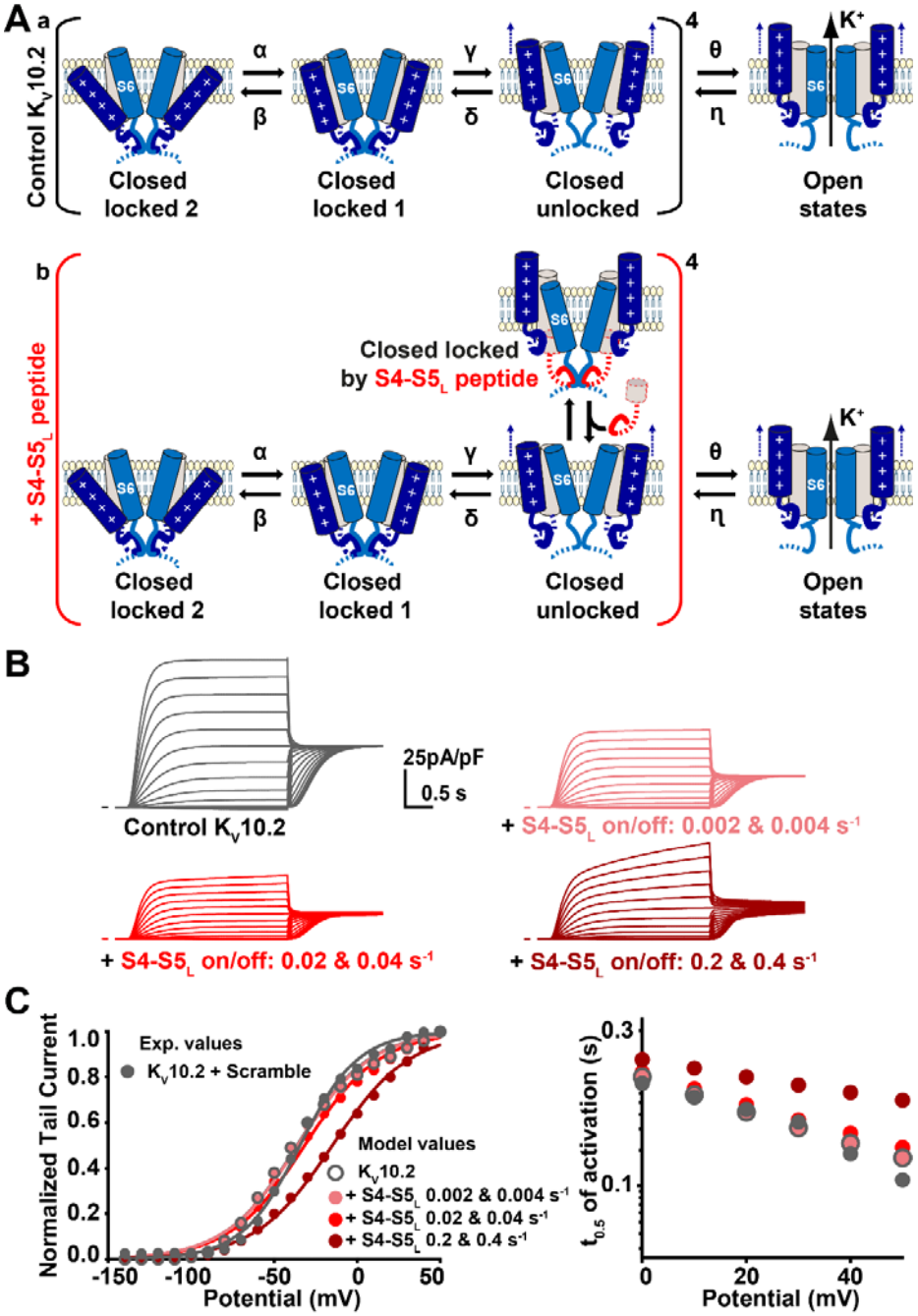

Figure 6: kinetic model of K_V10.2 and its interaction with the S4-S5$_L$ peptide. A: kinetic model schemes. This model is based on a previous work on KCNE1-KCNQ1 (23). ***a***: kinetic model in the absence of peptide, on which optimization has been performed (see experimental procedures). Optimized transition rates are presented in Table 1. ***b***: binding of exogenous S4-S5$_L$ locks the channel and prevents its opening. Peptides are supposed to interact with each monomer in the unlocked states. **B:** simulated currents during step protocols (same as in figure 5), in the absence (Ctrl) or the presence of S4-S5$_L$ peptide, at the indicated S4-S5$_L$ on/off rates. **C:** Grey filled circles: experimental activation curves and half-activation times in control condition. Other symbols: simulated values in the absence of peptide (control, open circles), or in the presence of peptides, at the indicated rates of peptide binding/unbinding.

Downloaded from http://www.jbc.org/ by guest on February 27, 2019

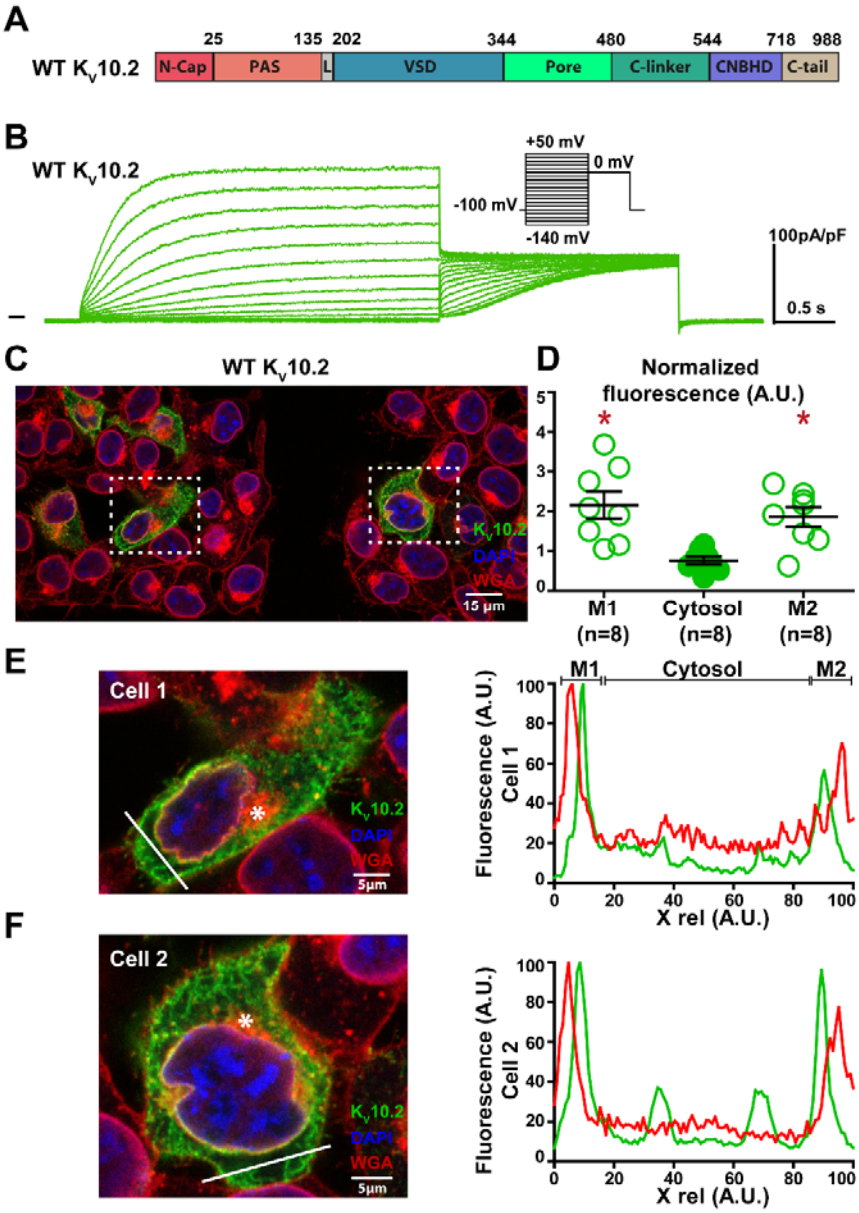

Figure 7: WT K_V10.2 characterization in transfected COS-7 cells. A: domains organization of the channel, showing the eag domain (N-Cap + PAS), a linker domain (L, also named proximal N-terminus), the voltage sensing domain (VSD), the pore domain, C-linker, CNBHD, and C-tail. **B:** representative, superimposed recordings of the WT K_V10.2-1D4 current. ***Inset*:** voltage protocol used (one sweep every 8 s). **C:** representative confocal immunostainings of WT K_V10.2-1D4 in transfected COS-7 cells (in green). WGA (wheat germ agglutinin) is used as a membrane marker (in red). Nuclei are stained with DAPI (in blue). Scale = 15 µm. **D:** mean ± sem fluorescence of K_V10.2 signal in plasma membrane (M1 and M2) and cytosol, as measured in E and F, normalized by the average K_V10.2 fluorescence. *p<0.05 versus cytosol, paired Student's t-test. **E & F.** ***Left:*** expanded view of two selected cells, showing the Golgi (stars) and the line used for the line plots shown in right. Lines have been placed as far as possible from the Golgi to generate accurate plasma membrane plots. ***Right:*** line plots of WGA (red) and K_V10.2 (green) at the level of the drawn lines in left. Higher K_V10.2 fluorescence densities are observed in the region of the plasma membrane.

Downloaded from http://www.jbc.org/ by guest on February 27, 2019

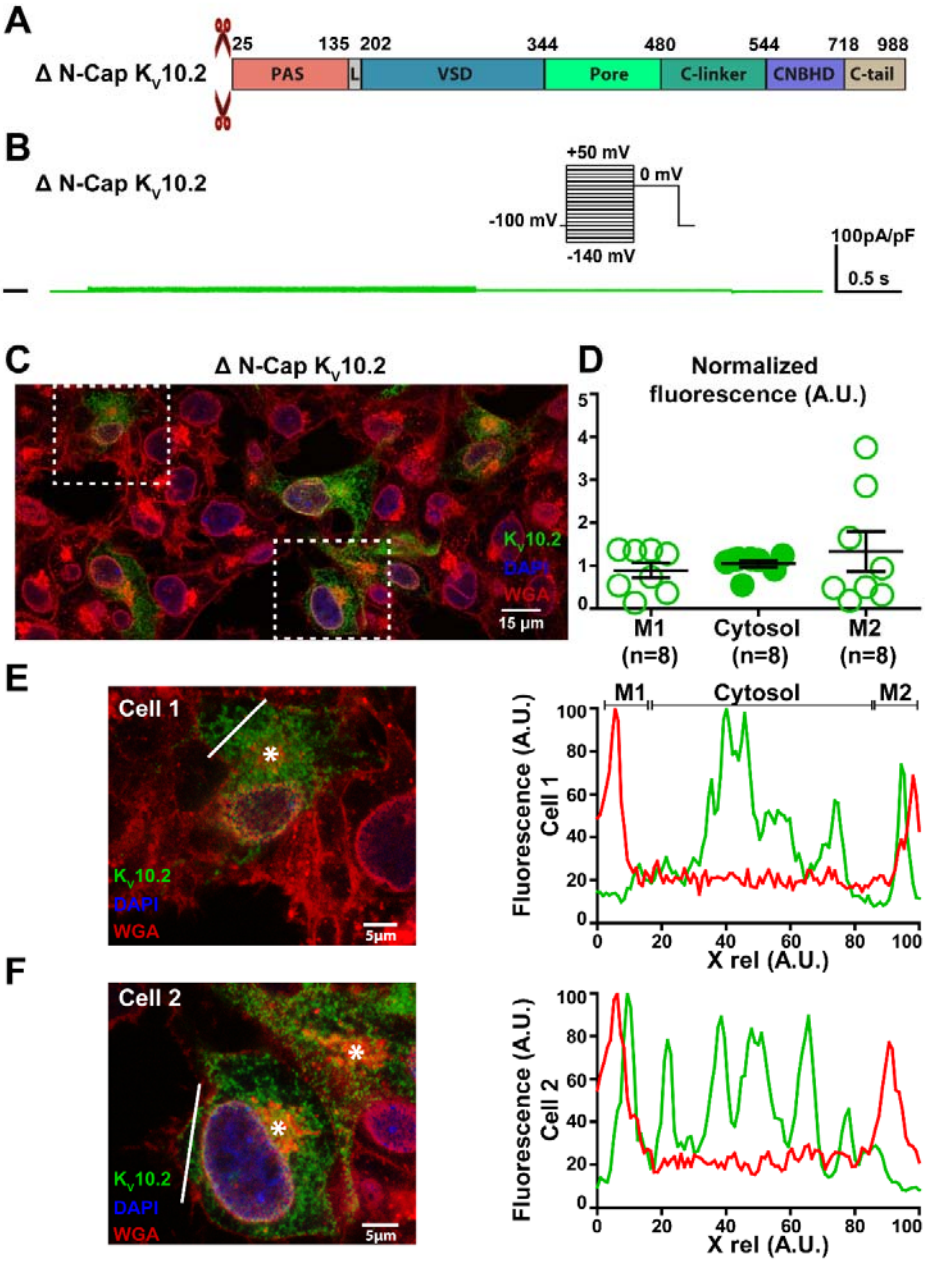

Figure 8: ΔN-Cap K_V10.2 characterization in transfected COS-7 cells. A: domains organization of the channel, showing the N-Cap deletion. **B:** representative, superimposed recordings of the ΔN-Cap K_V10.2-1D4 current. ***Inset*:** voltage protocol used (one sweep every 8 s). **C:** representative confocal immunostainings of ΔN-Cap K_V10.2-1D4 in transfected COS-7 cells (in green). WGA (wheat germ agglutinin) is used as a membrane marker (in red). Nuclei are stained with DAPI (in blue). Scale = 15 µm. **D:** mean ± sem fluorescence of K_V10.2 signal in plasma membrane (M1 and M2) and cytosol, as measured in E and F, normalized by the average K_V10.2 fluorescence. **E & F.** ***Left:*** expanded view of two selected cells, showing the Golgi (stars) and the line used for the line plots shown in right. Lines have been placed as far as possible from the Golgi to generate accurate plasma membrane plots. ***Right:*** line plots of WGA (red) and K_V10.2 (green) at the level of the drawn lines in left. Higher K_V10.2 fluorescence densities are not observed in the region of the plasma membrane, as opposed to the WT condition.

Downloaded from http://www.jbc.org/ by guest on February 27, 2019

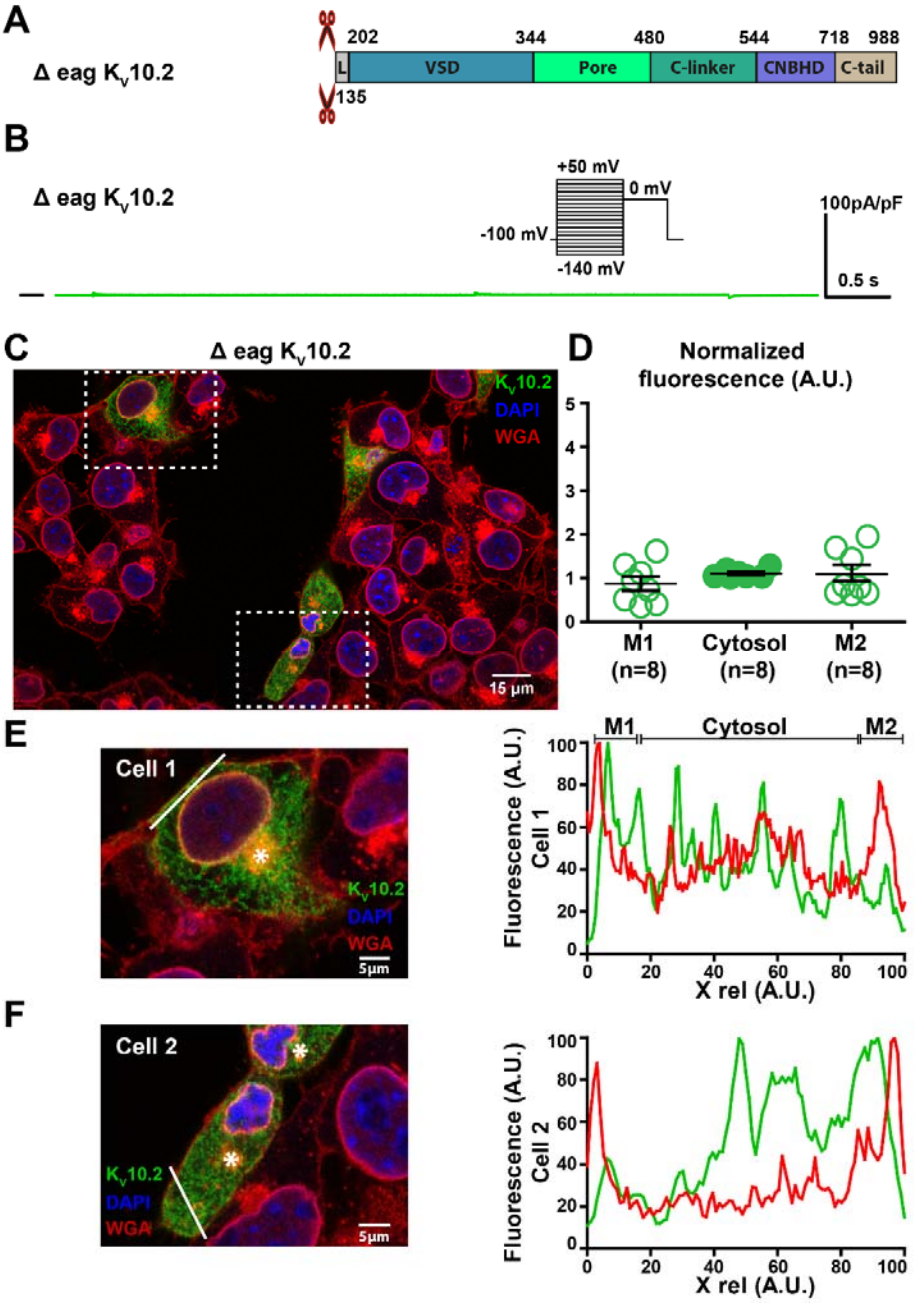

Figure 9: Δeag K_V10.2 characterization in transfected COS-7 cells. A: domains organization of the channel, showing the eag domain deletion. **B:** representative, superimposed recordings of the Δeag K_V10.2-1D4 current. ***Inset*:** voltage protocol used (one sweep every 8 s). **C:** Representative confocal immunostainings of Δeag K_V10.2-1D4 in transfected COS-7 cells (in green). WGA (wheat germ agglutinin) is used as a membrane marker (in red). Nuclei are stained with DAPI (in blue). Scale = 15 µm. **D:** mean ± sem fluorescence of K_V10.2 signal in plasma membrane (M1 and M2) and cytosol, as measured in E and F, normalized by the average K_V10.2 fluorescence. **E & F.** ***Left:*** expanded view of two selected cells, showing the Golgi (stars) and the line used for the line plots shown in right. Lines have been placed as far as possible from the Golgi to generate accurate plasma membrane plots. ***Right:*** line plots of WGA (red) and K_V10.2 (green) at the level of the drawn lines in left. Higher K_V10.2 fluorescence densities are not observed in the region of the plasma membrane, as opposed to the WT condition.

Downloaded from http://www.jbc.org/ by guest on February 27, 2019

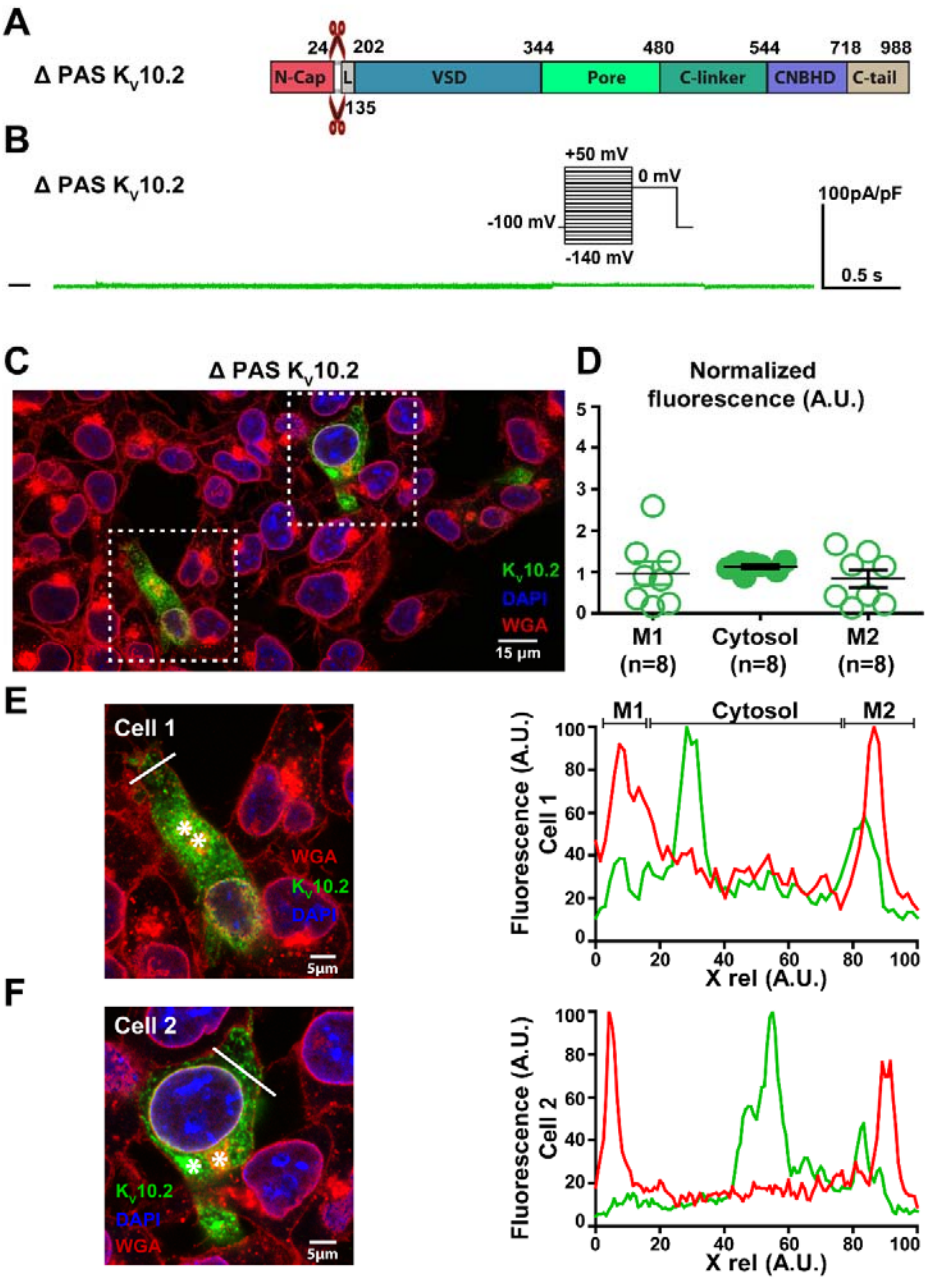

Figure 10: ΔPAS K_V10.2 characterization in transfected COS-7 cells. A: domains organization of the channel, showing the PAS domain deletion. **B:** representative, superimposed recordings of the ΔPAS K_V10.2-1D4 current. ***Inset*:** voltage protocol used (one sweep every 8 s). **C:** Representative confocal immunostainings of ΔPAS K_V10.2-1D4 in transfected COS-7 cells (in green). WGA (wheat germ agglutinin) is used as a membrane marker (in red). Nuclei are stained with DAPI (in blue). Scale = 15 µm. **D:** mean ± sem fluorescence of K_V10.2 signal in plasma membrane (M1 and M2) and cytosol, as measured in E and F, normalized by the average K_V10.2 fluorescence. **E & F.** ***Left:*** expanded view of two selected cells, showing the Golgi (stars) and the line used for the line plots shown in right. Lines have been placed as far as possible from the Golgi to generate accurate plasma membrane plots. ***Right:*** line plots of WGA (red) and K_V10.2 (green) at the level of the drawn lines in left. Higher K_V10.2 fluorescence densities are not observed in the region of the plasma membrane, as opposed to the WT condition.

Downloaded from http://www.jbc.org/ by guest on February 27, 2019

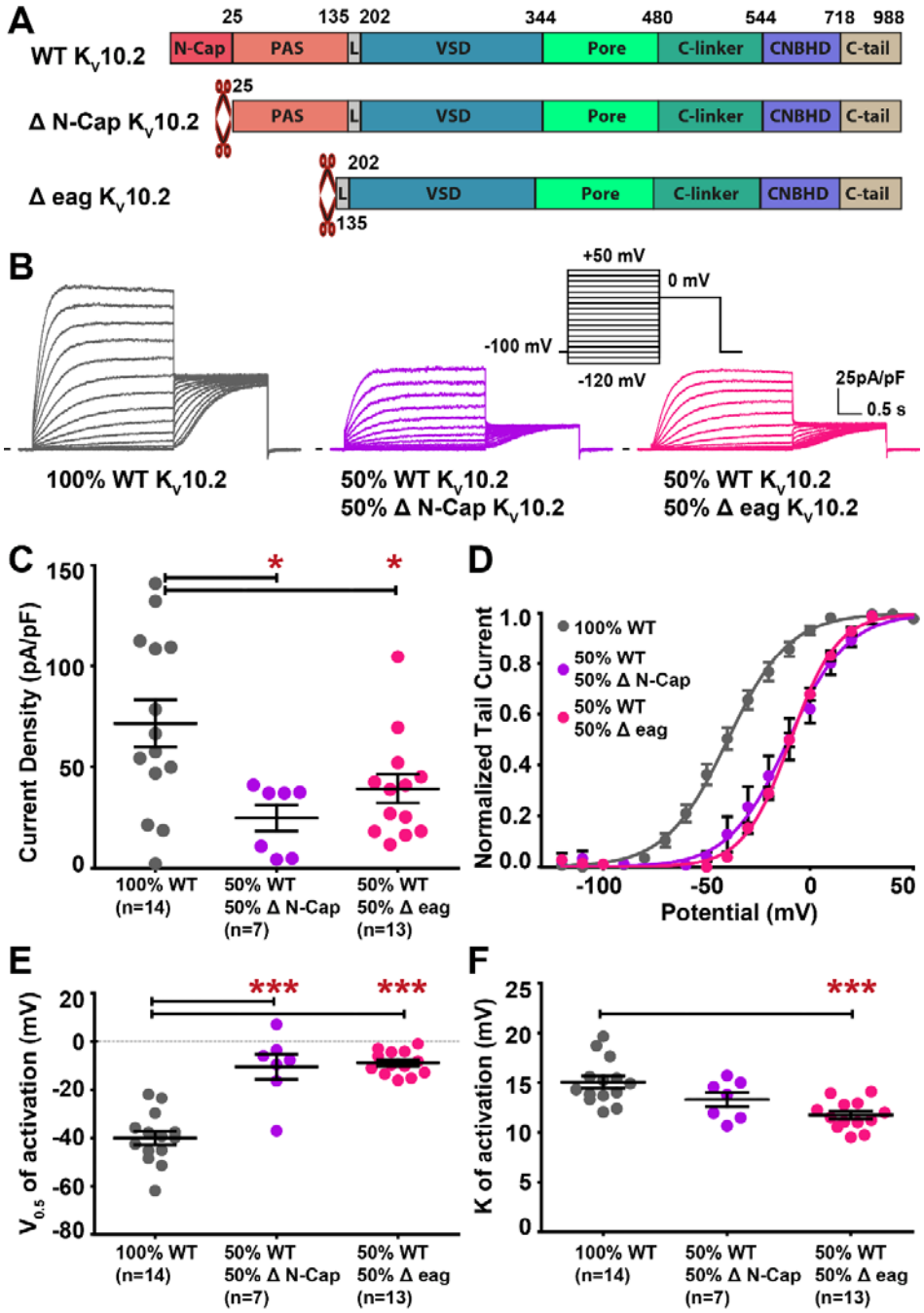

Figure 11: co-expression of WT and truncated K$_V$10.2 channels uncovers a right shift in the activation curve, as compared to WT channel. A: domain organization of WT and truncated channels. **B:** representative, superimposed recordings of COS-7 cells transfected with WT K$_V$10.2 channel (***left***), WT and ΔN-Cap K$_V$10.2 (***middle***) and WT and Δeag K$_V$10.2 (***right***). ***Inset*:** activation voltage protocol used (one sweep every 8 s). **C:** mean ± sem K$_V$10.2 maximum tail-current density, in the indicated conditions. *p<0.05 versus WT, Mann-Whitney test. **D:** activation curve in the indicated conditions. **E:** mean ± sem half-activation potential (V$_{0.5}$). ***p<0.001 versus WT, Student's t-test. **F:** mean ± sem activation slope (k). ***p<0.001 versus WT, Student's t-test.

Downloaded from http://www.jbc.org/ by guest on February 27, 2019

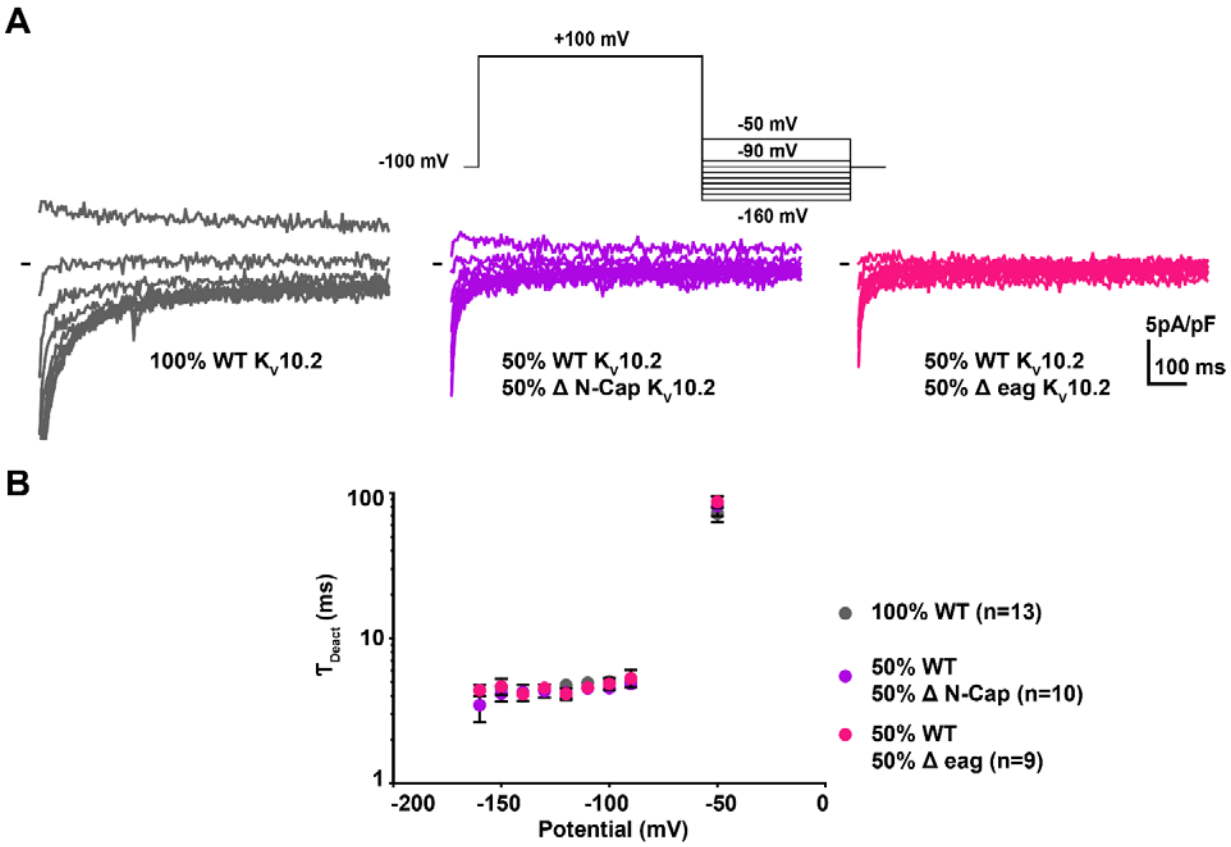

Figure 12: co-expression of WT and truncated K$_V$10.2 channels is not associated with changes in deactivation kinetics, as compared to WT channel. A: representative, superimposed recordings of COS-7 cells transfected with WT K$_V$10.2 channel (***left***), WT and ΔN-Cap K$_V$10.2 (***middle***), and WT and Δeag K$_V$10.2 (***right***). ***Upper inset*****:** deactivation tail voltage protocol used (prepulse duration 3s, one sweep every 7 s). **B:** mean ± sem K$_V$10.2 deactivation time constant, obtained from a mono-exponential fit of the deactivating current.

Downloaded from http://www.jbc.org/ by guest on February 27, 2019

Voltage-dependent activation in EAG channels follows a ligand-receptor rather than a mechanical-lever mechanism

Olfat A. Malak, Grigory S. Gluhov, Anastasia V. Grizel, Kseniya S. Kudryashova, Olga S. Sokolova and Gildas Loussouarn

J. Biol. Chem. published online February 26, 2019

Access the most updated version of this article at doi: 10.1074/jbc.RA119.007626

Alerts:
- When this article is cited
- When a correction for this article is posted

Click here to choose from all of JBC's e-mail alerts

Downloaded from http://www.jbc.org/ by guest on February 27, 2019